Investigation of natural circulation capabilities of the Molten Salt Fast Reactor

by

David van Nijen

in partial fulfillment of the requirements for the degree of

Bachelor of Science
in Applied Physics

at the Delft University of Technology,
to be defended publicly on Friday July 12, 2018.

student number: 4481933

Supervisor:	ir. M. Tiberga	
Thesis committee:	Dr. ir. D. Lathouwers	TU Delft
	Dr. ir. M. Rohde	TU Delft

TU Delft Delft University of Technology

Abstract

The Molten Salt Fast Reactor (MSFR) is a nuclear reactor that should be able to produce energy in a safer, more reliable and more sustainable way than the currently most used Light Water Reactor (LWR). For example, the MSFR produces nuclear waste that is less long lived than that of the LWR. Furthermore, in case of overheating the freeze plugs at the bottom of the MSFR melt, which will make sure that the salt is able to flow freely to cooled emergency tanks.

If the pumps of an MSFR stop working, the reactor would be shut down immediately to avoid overheating. However, there would still be delayed heat production due to decay of the fission products present in the molten salt. Natural circulation is a purely passive mechanism that can cool down the reactor, even when the pumps are out of order. In this report, the possibility to rely on natural circulation to remove heat during such an accident is described. Furthermore, an investigation about the influence of the height of the heat exchanger on the natural circulation capabilities is treated. The investigations were performed with a Finite Element CFD code able to simulate the flow of the molten salt in the MSFR.

From the simulations, it can be concluded that the MSFR is able to cool itself down in case the pumps stop working and the reactor shuts down at the same moment. In the first 5s after the accident, the flow through the sectors is disturbed, but it gradually reestablishes itself through natural circulation. Overheating of the fuel loop does not occur, the maximum fluid temperature does not even increase after the pumps stop working.

The height of the heat exchanger slightly influences the natural flow capabilities of the MSFR. If the heat exchanger is raised with 13 cm relative to the normal MSFR geometry, the molten salt flow velocity will be up to 14.5% higher than if it is lowered by 13 cm. However, in most regions of the fuel loop the natural flow velocity does not differ more than 3.8% for the different heights of the heat exchanger. The difference in flow velocity does not result in temperature differences of more than 3.5K between the geometries with different heights of the heat exchanger. Hence, the experiment shows that in- or decreasing the heat exchanger height with 13 cm does not have a significant impact on the natural cooling capabilities of the MSFR.

Contents

List of Figures

List of Tables

1

Introduction

Nuclear reactors generate a substantial amount of the energy used every day without emission of CO_2, which they are able to do by initiating and controlling a self-sustained nuclear chain reaction. Nowadays, the Light Water Reactor (LWR) is the most commonly used reactor type. It uses enriched Uranium as a fuel, which is a type of Uranium in which the percent composition of U-235 is increased to about 3%. The LWR was relatively easy to build 50 years ago, but even at that time it was not the most safe nor the most efficient type of reactor. One of the main downsides of nuclear reactors is that they produce nuclear waste that has to be kept out of the reach of humans. Furthermore, the trust of society in nuclear energy has decreased due to some nuclear reactor disasters, including those in Fukushima and Chernobyl.

The Generation IV International Forum (GIF) was formed in 2000 to begin an international collaboration in the development of a new generation of nuclear energy systems. GIF is a collaboration between 14 countries that aims to develop nuclear systems that will be able to respond to the increasing energy needs of the world. The research and development of six selected reactor types should in the future be able to respond to the economic, environmental and social requirements of the 21st century.

This report treats one of the Generation IV Reactors, the Molten Salt Fast Reactor (MSFR). The MSFR should be able to produce energy in a safer, more reliable and more sustainable way than the LWR. It uses U-233 as a fuel instead of U-235, which results in nuclear waste that is much less long lived than that of the LWR. Furthermore, the freeze plugs at the bottom of the MSFR melt in case of overheating, which makes sure that the salt is able to flow freely to cooled emergency tanks [1]. This thesis is a part of the Safety Assessment of a Molten salt Fast Reactor (SAMOFAR) project, which was started in 2015 to deliver experimental proof of several key safety features of the MSFR. The aim of this thesis is to describe the possibility to rely on natural circulation to remove decay heat during accidents, which is a purely passive mechanism that contributes to the safety of the MSFR.

1.1. The Molten Salt Fast Reactor

This section covers the basic principles of the MSFR that are relevant for this thesis.

1.1.1. Overview

A general overview of the Molten Salt Fast Reactor (MSFR) can be seen in Figure 1.1. In the fuel circuit, heat is generated by the fission of heavy nuclei. The function of the intermediate circuit is to transport this generated heat to the energy conversion circuit, where it can be converted into electricity. This report will focus on the fuel circuit only [2].

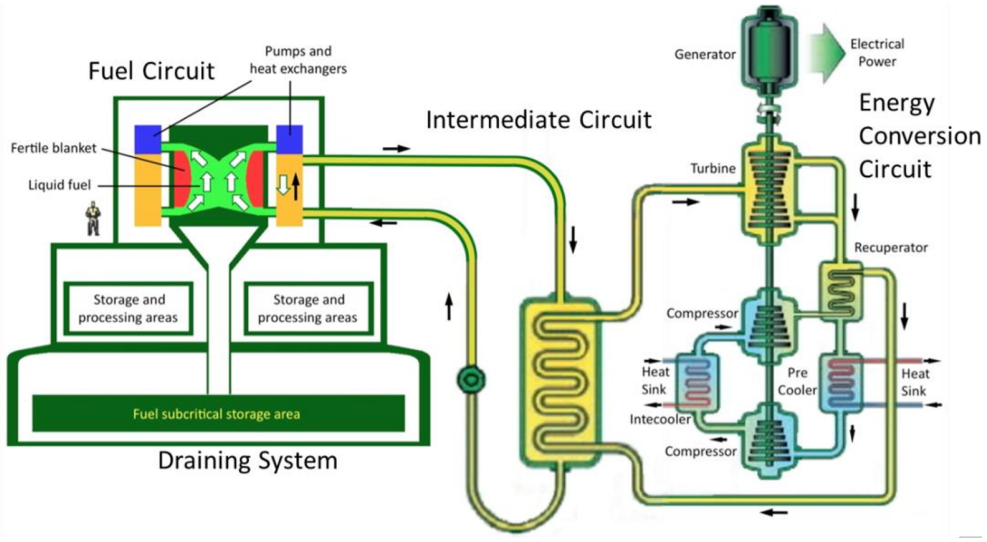

Figure 1.1: A schematic representation of the complete MSFR [2].

1.1.2. Fuel characteristics

The fluid of the fuel circuit consists of a fuel dissolved in a liquid fluoride salt. The intermediate fluid consists of a liquid metal or a molten salt. The two candidate initial fuel salt compositions selected for the fuel circuit are

1. LiF-ThF_4-^{233}U (77.5-20-2.5 mol%);
2. LiF-ThF_4-$^{enr}UF_4$-(Pu-MA)F_3 (77.5-6.6-12.4-3.6 mol%) .

In order to prevent the molten salt from solidifying, the fuel temperature should be kept above the melting temperature of 831K. Furthermore, the fuel temperature should stay below 1473K to prevent the salt from causing structural damages [3]. In order to have a safety margin from both the melting temperature and the temperature where the salt causes structural damages, the mean operating temperature of the fuel is chosen at 998 K [2].

1.1.3. Nuclear reactions

If neutrons are fired upon an unstable nucleus, this results in a fission reaction. In a nuclear reactor, energy is released during the fission of heavy nuclei in a controlled chain reaction. The released energy consists mostly of kinetic energy of the fission products, which are slowed down due to viscous forces. The released fission products are often unstable as well, which means they decay and release energy (mostly in the form of γ-rays). Eventually the energy of the fission reactions is converted into heat [4]. The salt composition in the MSFR consists of Th-232. This element is not fissile and cannot be used as fuel in a nuclear reaction. However, if it captures a neutron the Th-233 product decays (first quickly to Pa-233 and then) with a half-life of about one month to U-233. This is an artificial isotope of Uranium that is highly fissile and is suitable as fuel in the MSFR. To sustain a fission reaction, on average one of the three released neutrons of the fission is needed to convert the next Th-232 to U-233 and another one is needed to induce the fission of the U-233.

The usage of Th-232 in the fuel has two main advantages. First, it is an element that is three times more abundant in nature than Uranium, which means that it can be used to generate energy on a large scale. Second, using U-233 as a fuel produces much less long-lived nuclear waste than the enriched U-235 of the LWR. On the long term, the main part of the radiotoxicity of spent nuclear fuel of an LWR is caused by the actinides Plutonium and Americium that are present. U-233 needs four neutron capture reactions before it can decay to Plutonium and Americium, whereas the U-238 that is present in an LWR only needs one. Hence, the long living actinides Plutonium and Americium are produced in much smaller quantities in an MSFR with U-233 than in the LWR with enriched U-235 as a fuel [1].

1.1.4. Fuel circuit

An overview of the fuel circuit of the MSFR is shown in Figure 1.2. The fuel is heated up in the reactor core by fission reactions at a nominal power of 3 GW_{th}. The fuel salt temperature rise in the core is

around 100 K (from 948±25 K to 1048±25 K). The fluid is pumped through sixteen different channels called *sectors*. All of these sectors contain their own heat exchangers so that the heat of the fuel circuit can be transferred to the intermediate circuit. The sectors are evenly distributed around the core, which can be seen in Figure 1.3. The fuel flows from the top of the core through the sectors, after which it enters the core again from below. Here, it rises to the top of the core while heating up [2].

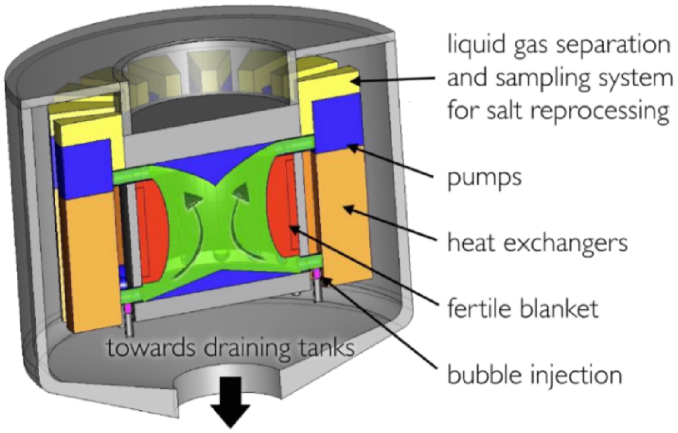

Figure 1.2: Schematic representation of the MSFR fuel circuit. [2]

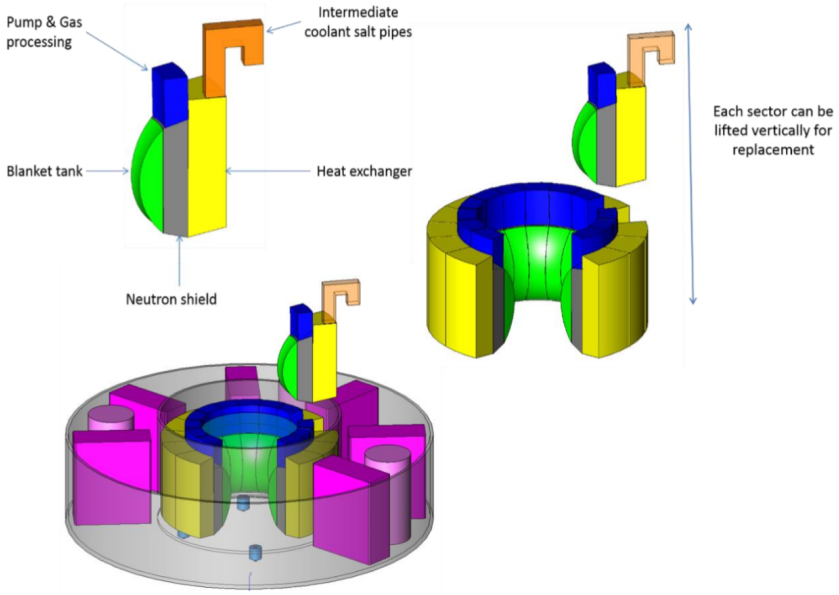

Figure 1.3: Schematic representation of the sectors placed around the core. [2]

1.1.5. Delayed heat production

Immediately after reactor shutdown the decay heat reduces to about 6% of its nominal power, after which it gradually decreases over time. The reason of this delayed heat production is that there are still unstable fission products present in the salt after reactor shutdown, which release energy at the moment that they decay (mostly in the form of β^- and γ rays). The delayed heat production is plotted as a function of time in Figure 1.4 [4]. It can be seen that it takes 100s before the delayed heat production reduces from 6% to 3%.

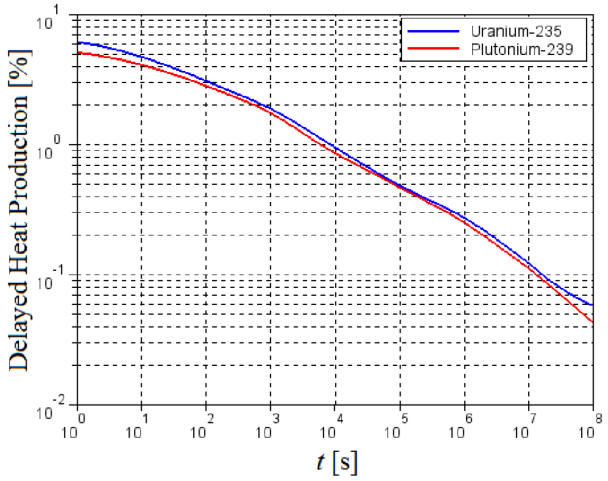

Figure 1.4: Decay heat after reactor shutdown as a function of time. Immediately after the shutdown the decay heat reduces to 6% of its nominal power, which reduces further to about 3% after 100s. [4]

1.2. Thesis' focus and layout

This bachelor thesis is a part of the European project SAMOFAR (Safety Assessment of the MOlten salt FAst Reactor), whose goals include proving the innovative safety aspects of the MSFR by numerical simulations. One of these aspects is the possibility to rely on natural circulation to remove heat during accidents. A possible accident that can happen is a loss of flow due to an outbreak of the pumps, which would decrease the capacity to remove fission heat. If such an event were to happen, the reactor would be shut down to avoid overheating. However, there would still be delayed heat production due to the fission products that are already present. Natural circulation is a purely passive mechanism that can cool down the reactor, even when the pumps are out of order. This thesis project describes an investigation of the natural circulation capabilities of the MSFR:

- The thesis aims to describe to what extent natural circulation is able to remove delayed heat production in case the pumps stop working;
- Furthermore, the influence of the height heat exchanger on the natural circulation capabilities is described.

The investigation was performed with a Finite Element Computational Fluid Dynamics code able to simulate the flow of the molten salt in the MSFR, which has been developed by The Reactor Physics and Nuclear Materials section of Delft University of Technology.

The remainder of the thesis is structured as follows. Chapter 2 describes theory about natural convection, fluid mechanics, and computational fluid dynamics. This is followed by an explanation of how the simulations were performed in chapter 3. In chapter 4, an error that was encountered during the simulations is treated. In chapter 5 the results of the simulations are discussed, and in chapter 6 the conclusions are presented.

2

Theory

In this chapter the theoretical background of the research is covered. The first section is meant to provide some insight into natural convection in fluids; the second section describes fluid mechanics theory that is relevant for the project, and the third and final section treats how the physics are numerically approximated in order to predict fluid flow accurately.

2.1. Physics of natural convection

2.1.1. Buoyancy force

The buoyancy force is the upward force exerted on an object submerged in a fluid. The equation for buoyancy force F_B is

$$F_B = \rho_f V_{object} g. \tag{2.1}$$

In this equation, ρ_f is the density of the fluid, V_{object} is the volume of the submerged object and g is the gravitational acceleration. Every object submerged in a fluid is also subject to the gravitational force. The net force on the object is the sum of the gravitational force and the buoyancy force. If an object with a density ρ_o different from ρ_f is submerged in a fluid, the buoyancy force will make the object rise if ρ_o is smaller than ρ_f, and it will make the object sink if ρ_o is larger. If the submerged object has a density of ρ_f, the buoyancy force and the gravitational force cancel each other out and the object will stay in place [5].

2.1.2. Natural convection

The density of the working fluid in the MSFR has a negative derivative with temperature:

$$\frac{\partial \rho_f}{\partial T_f} < 0. \tag{2.2}$$

This means that the higher the fluid temperature is, the lower the fluid density is [6]. In an MSFR, the fluid is subject to both heating and cooling, leading to density differences in the fluid. If a part of a fluid expands due to heating, its volume will increase while its mass stays the same. This means that the buoyancy force on this part of the fluid will increase, while the gravitational force will remain the same. Hence, if a part of a fluid has a higher temperature than the surrounding fluid, it will rise due to an increased buoyancy force; likewise, colder fluids will sink.
Natural convection in a fluid is an interaction between driving buoyancy forces and viscous resistance forces. In the fuel loop of an MSFR, natural convection is a result of the heat that is generated by fission reactions in the core and the cooling that is taking place in the heat exchangers.

2.2. Fluid Mechanics

2.2.1. Navier-Stokes equations

A constitutive equation describes the relation between the stress and deformation in a continuum. Cauchy's equation relates the acceleration to the net force at a point and holds for any continuum.

By filling in the constitutive equation for Newtonian fluids into Cauchy's equation, the Navier-Stokes equations are obtained.
The Navier-Stokes equations are partial differential equations that describe the flow of fluids. They express the second law of Newton for a unity volume of a fluid, which means that they describe dynamical expressions of the net force on a fluid part.
The general form of the Navier-Stokes equation is often simplified by making assumptions. The incompressible Navier-Stokes equations in vector form are:

$$\begin{aligned} \nabla \cdot \mathbf{u} &= 0 \\ \rho \frac{D\mathbf{u}}{Dt} &= -\nabla p + \mathbf{f} + \mu \nabla^2 \mathbf{u} \end{aligned} \tag{2.3}$$

In these equations **u** is the velocity vector, p is the pressure, **f** is a known body force (for example gravity $\mathbf{f}_g$), and μ is the dynamic viscosity. The equation is written in the Lagrangian form, which includes a material derivative. This type of formulation describes the motion of some chosen particles in a fluid. Equation 2.3 can also be written in the Eulerian form:

$$\rho \left(\frac{\partial \mathbf{u}}{\partial t} + (\mathbf{u} \cdot \nabla)\mathbf{u} \right) = -\nabla p + \mu \nabla^2 \mathbf{u} + \mathbf{f} \tag{2.4}$$

The Eulerian formulation describes the flow of a fluid through a control volume [8].

2.2.2. Boussinesq approximation

In the Boussinesq approximation the density changes in a fluid can be neglected, except in the body force term. Furthermore, this approximation treats the other properties of the fluid (namely, dynamic viscosity μ, thermal conductivity λ and heat capacity c_p) as constants.
The Boussinesq approximation is only applicable to fluids where the flow satisfies the following conditions:

1. The Mach number of the flow needs to be smaller than 0.3. The Mach number is defined as $\frac{u}{c}$, in which u is a typical measure of the flow speed and c is the speed of sound in the medium. The flow speeds that are normally achievable in liquids are much smaller than the speed of sound.

2. The vertical scale of the flow needs to be $L << \frac{c^2}{g}$. If the vertical scale of the flow is too large, the hydrostatic pressure (pressure due to weight of fluid column above it) variations can cause large changes in density.

The flows in a MSFR satisfy these conditions, which means that the Boussinesq approximation can be applied [8].

2.2.3. Pressure Drop

When a fluid is flowing through a pipe, the pressure at the inlet is usually higher than the pressure at the outlet. This is a result of friction between different layers of the fluid and between the fluid and the pipe wall. Because the fluid loses energy due to this friction, there is a pressure loss. This phenomenon does not only occur in pipes, but in fluids that are flowing in any geometry. The pressure drop can be defined by the Darcy-Weisbach equation:

$$\frac{\Delta p}{L} = \frac{1}{2} \frac{f_d}{D_h} \rho \langle v \rangle^2 . \tag{2.5}$$

In this equation, Δp is the pressure loss, L is the length of the pipe, v is the velocity of the fluid and f_d is the Darcy friction factor. The hydraulic diameter D_h makes it possible to use the Darcy-Weisbach equation on non-cylindrical geometries and is defined as $\frac{4A}{S}$, where A is the area through which the fluid flows and S is the wetted perimeter.

In equation 2.5, the Darcy friction factor f_d of a cylindrical pipe is dependent on the Reynolds number (Re) of the flow. For laminar flows ($Re < 2000$), f_d is $\frac{64}{Re}$. For turbulent flows ($4000 < Re < 10^5$), f_d is $0.316 Re^{-1/4}$. These formulas cannot be used directly in the MSFR geometry, but they provide some

intuition about the order of magnitude of the friction factor. It should be noted that the Fanning friction factor is also often used. This is nothing but the Darcy friction factor divided by four [7].

In the MSFR, pressure drops mainly occur in the heat exchangers because of their relatively narrow channels. The larger the pressure drop, the better the pump performance should be to achieve the same fluid flow. Furthermore, the larger the pressure drop is, the harder it is to establish natural circulation flow. For a higher Δp the temperature difference should be higher to make the fluid flow naturally at the same velocity [2].

2.3. Computational Fluid Dynamics

The (incompressible) Navier-Stokes equations cannot be solved for flows in complex geometries. Computational Fluid Dynamics (CFD) is a science that produces quantative predictions of fluid-flow phenomena based on the conservation laws governing fluid motion. In CFD, the differential equations are solved numerically in order to simulate the flow. The solutions that CFD provides are approximations of the real solutions [8].

2.3.1. Finite Element Method

The Finite Element Method (FEM) is a numerical method for partial differential equations. In this method, differential equations are solved by subdividing the domain into smaller, simpler parts called finite elements. The FEM has flexibility to handle complex geometries [9]. Given the complex geometry of the MSFR loop, the FEM approximation is used to discretize the Navier-Stokes equations [6].

2.3.2. Weak formulation

Before applying the FEM, a *weak formulation* of a differential equation has to be derived. In order to demonstrate how this works, the following Partial Differential Equation (PDE) is considered:

$$\begin{cases} \nabla \cdot [\lambda \nabla c(\mathbf{r})] = f(\mathbf{r}) & \text{with } \mathbf{r} \in \Omega \\ c = g & \text{on boundary } \partial\Omega \end{cases} \tag{2.6}$$

The weak formulation can be derived by multiplying the differential equation by a variational function w and integrating over the domain Ω where the problem is defined. This variational function is a function in variational space, which implies that the condition $w = 0$ on boundary $\partial\Omega$ is satisfied. The trial solution c to the differential equation itself is defined in trial function space S, not in variational space. A function in trial function space satisfies the same boundary condition of the PDE that it is equal to g on the boundary $\partial\Omega$.

Once the PDE has been multiplied by this variational function w, the second derivative terms can be rewritten by applying integration by parts in combination with the Gauss divergence theorem. The final step to arrive at the weak formulation is to apply the boundary conditions. Solutions to the strong and the weak form of a differential equation are equivalent, there is no approximation involved in the derivation of the weak formulation [8].

2.3.3. Continuous Galerkin method

For most descriptions of fluid dynamics, the Galerkin finite element formulation is used. The trial function space and variational space are approximated by corresponding finite dimensional spaces S^N and V^N with characteristic grid sizes N. To arrive at the Galerkin formulation, all functions of the differential equations have to be expressed in variational space. In order to do this, a new trial function $v^N(\mathbf{r}) = c^N(\mathbf{r}) - c_0^N(\mathbf{r})$ in variational space is defined, where $c_0^N(\mathbf{r})$ is a specific function that satisfies the condition $g^N(\mathbf{r}) = g$ on $\partial\Omega$ [8].
In the Galerkin method the solution v to this differential equation is approximated by a linear combination of basis functions:

$$v^N(\mathbf{r}) = \sum_{j=1}^{N} c_j \phi_j(\mathbf{r}) \tag{2.7}$$

where ϕ_j are chosen basis functions and the parameters c_j are to be determined. The solution $c^N(\mathbf{r})$ can be expressed in trial function space S again by adding the term $c_0(\mathbf{r})$ (for which $c_0(\mathbf{r}) = g$ on $\partial\Omega$)

to $v^N(\mathbf{x})$:

$$c^N(\mathbf{r}) = \sum_{j=1}^{N} c_j \phi_j(\mathbf{r}) + c_0(\mathbf{r}) \tag{2.8}$$

The approximated solution $c^N(\mathbf{r})$ can be substituted into the Galerkin formulation of the problem. Also the variational function w is approached with the same basis functions ϕ_j, but with different coefficients. Therefore, the PDE becomes a system of N linear equations with N unknowns. A mesh generator can subdivide a region into small elements called 'finite elements'. In each of these elements the unknown function is approximated by a linear combination of the basis functions ϕ_j [10]. The integrals over the region are splitted into integrals over the elements. In these integrals, only the basis functions corresponding to the nodal points in the element have a non-zero contribution to the integrals. These integrals can be computed and stored in an element matrix, with which the solution $c(\mathbf{r})$ to the differential equation can be reconstructed [8].

2.3.4. Discontinuous Galerkin Method

High order continuous Galerkin methods offer geometrical flexibility and high parallel efficiency. However, the implementation of these methods is rather complex and if the mesh elements are not sufficiently fine they can become unstable. In Finite Volume methods the node points in a mesh are surrounded with a volume. With the divergence theorem the Partial Differential Equations (PDEs) that contain a divergence term are converted to surface integrals, which are then evaluated as fluxes at the surfaces of each finite volume. The FV methods are locally conservative because the flux entering a volume is identical to that leaving the adjacent volume.

The Discontinuous Galerkin (DG) method is able to combine the advantages of Continuous Galerkin and Finite Volumes, because it is based on CG, where the surface integrals are evaluated as fluxes. The DG method offers robustness at high Reynolds numbers flows, geometric flexibility, high-parallel efficiency and local conservativity [11]. The Reactor Physics and Nuclear Materials section has chosen to discretize the Navier-Stokes equations with the Discontinuous Galerkin (DG) method.

Because DG belongs to the Finite Elements methods, DG requires PDEs to be cast into a weak formulation. However, in discontinuous methods the discrete functions do not have to be continuous between neighbouring elements. Continuity can still be achieved by introducing flux, jump and and/or penalization terms on the faces between neighboring elements [12]. The Discontinuous Galerkin Method leads to FV treatment of the face integrals arising from the diverge terms after the use of the Gauss theorem, which results in an increased stability compared to CG methods. A face integral derived from a discretization is evaluated with a suitable numerical flux which must be continuous, consistent and conservative.

3

Simulation method

The following chapter describes how the simulations were performed. In the first section it is explained how a 3D-mesh of the fuel loop geometry was created. The properties of the molten salt and the fuel circuit that were used for the simulations are treated in the second section. In the third and final section the performed simulations are described in detail.

3.1. Creating a mesh of the fuel loop

In order to perform the simulations, a mesh of the geometry of the MSFR fuel circuit had to be created first. The program chosen to create the mesh is called Gmsh, which is an open-source three-dimensional finite element grid generator [13]. The complete fuel circuit consists of a core with 16 sectors. However, the mesh used for the simulations only consists of one sector with one-sixteenth slice of the core. If symmetry conditions are assigned to the sides of the core slice, the experiment gives realistic results with reduced computational effort.

At the start of the project, a 3D model of the MSFR fuel loop developed in previous studies was already available [14]. Because it was a research goal to investigate the influence of the height of the heat exchanger on the natural circulation capabilities, it would benefit the project if the geometry of the mesh could be adjusted easily. For this reason the fuel loop was created from scratch in Gmsh instead of importing a 3D STEP-file of the previously developed fuel loop geometry.

Creating a grid in Gmsh starts with defining points and lines between the points. In Figure 3.1 the lines and points of both the imported 3D-model and the created geometry are shown. As can be seen, the two geometries have approximately the same dimensions, but the created mesh consists of less points (124) than the imported 3D-model (948). Furthermore, it can be seen that the 3D-model consists of more different adjacent volumes (32) than the created mesh (9); for example, the core of the fuel loop consists of one volume, whereas the core of the 3D model consists of 6 different adjacent volumes. The created geometry is a slightly less accurate description of the developed fuel loop geometry than the imported model. Nevertheless, the fact that it is more easily adjustable makes it suitable for the simulations that are performed for this project.

The dimensions of the fuel loop geometry are shown in Figure 3.2. The z=0 and r=0 point was taken exactly in the middle of the core. Furthermore, the location of the pump and the heat exchanger during the simulations are indicated in Figure 3.3. In the next section it will be explained how the pump and the heat exchanger were simulated.

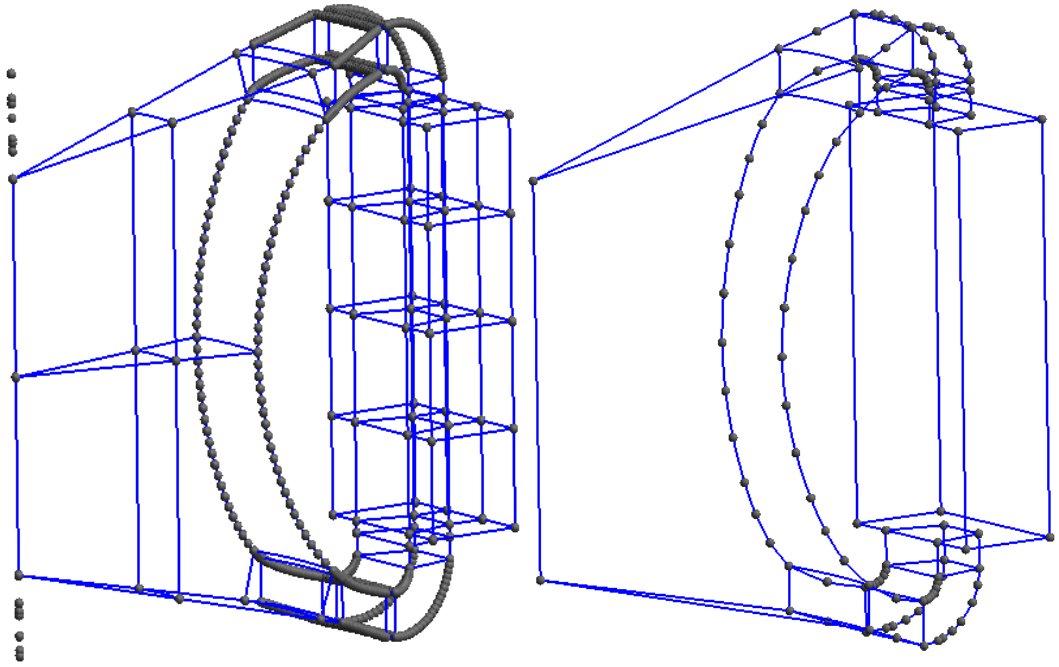

(a) Previously developed 3D model (b) The created fuel loop geometry

Figure 3.1: The points and lines of the previously developed 3D model of the fuel loop (a) and of the geometry that was created for this project (b).

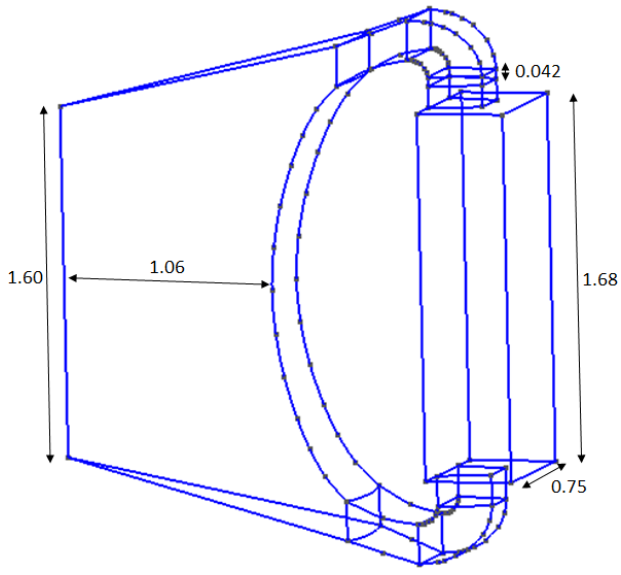

Figure 3.2: Mesh dimensions (m)

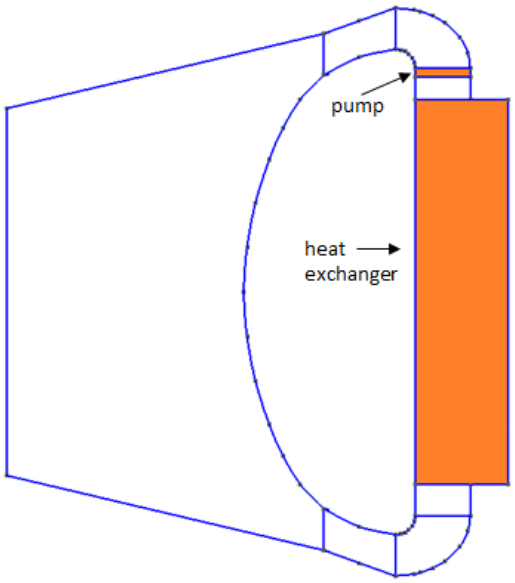

Figure 3.3: Pump and heat exchanger location indicated

The mesh was created by filling the fuel loop geometry with tetrahedral shaped elements. Although the results of simulations get more accurate for a finer mesh, the simulations require a higher computational effort. For this experiment it was chosen to fill the mesh with 13369 tetrahedra, resulting in an average size of 88 cm^3 per element. This mesh size preserves a balance between computational effort and accurate results. The used mesh can be seen in Figure 3.4.

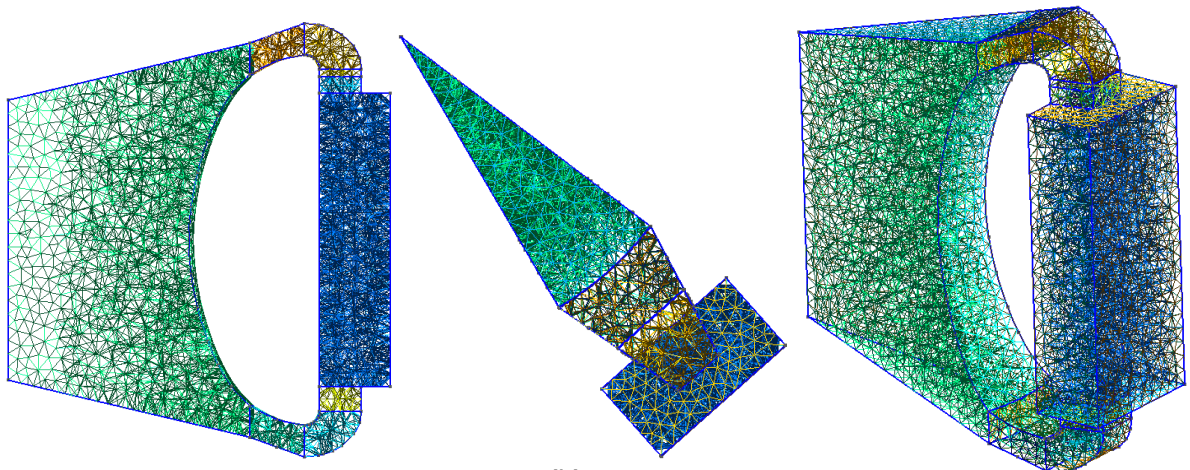

(a) Side (b) Up (c) Overview

Figure 3.4: The mesh of the fuel circuit geometry that was created in gmsh.

3.2. Simulations of the molten salt flow

For the simulations of the molten salt flow, the Discontinuous Galerkin flow code (DG-flow code) of the Reactor Physics and Nuclear Materials section of Delft University of Technology has been used.

3.2.1. Physicochemical properties of the molten salt

The properties of the molten salt taken from EVOL deliverable 2.6 [16] are summarized in the table 3.1.

Table 3.1: Properties of the molten salt [16].

	Formula	Validity range (K)
Density ρ (g/cm3)	$4.049 - 8.82 \cdot 10^{-4}(T(K) - 1008)$	893 - 1123
Kinematic viscosity ν (m2/s)	$5.54 \cdot 10^{-8}$ exp$(3698/T(K))$	898 - 1119
Dynamic viscosity μ $(Pa \cdot s)$	$\rho \cdot 5.54 \cdot 10^{-5}$ exp$(3698/T(K))$	898 - 1119
Thermal Conductivity λ (W/m/K)	$0.928 + 8.397 \cdot 10^{-5} \cdot T(K)$	891 - 1020
Calorific capacity C_p (J/kg/K)	$-1111 + 2.78 \cdot T(K)$	867 - 907

Because the DG-flow code was not yet able to handle turbulence at the time these simulations were performed, the flow of the molten salt had to be kept the laminar region. Because flows in a real MSFR are often turbulent, the material properties had to be adapted to maintain a laminar flow. In the simulations the kinematic viscosity ν was defined as $5.54 \cdot 10^{-4} exp(3698/T(K))$ and the thermal conductivity λ as $(0.928 + 8.397 \cdot 10^{-5} \cdot T(K)) \cdot 10^4$. The remaining material properties were taken from table 3.1, which results in both a laminar flow and a realistic Prandtl number.

3.2.2. Power source

In this project the DG-Flow code was not coupled to a radiation transport code to simulate the nuclear reactions in the MSFR fuel loop. The generated heat of the nuclear reactions were approximated by imposing the following power source [17] at the center of the core:

$$Q_{pow}(r,z) = \begin{cases} Q'''_{pow_0} \cos\left(\frac{z}{H} \cdot \frac{\pi}{2}\right) J_0\left(\frac{r}{R} \cdot \rho_0\right) & \text{, if } r \leq R \text{ and } |z| \leq H; \\ 0, & \text{, otherwise.} \end{cases} \tag{3.1}$$

In this equation, z is the vertical, and r the horizontal distance from the center of the core. J_0 is a Bessel function of the first kind, and Q'''_{pow_0} is a constant that should make sure that the core power output of the MSFR is $3GW$. This nominal power was chosen in the SAMOFAR project [2]. The evaluation of the integral $Q'''_{pow_0} * \int_0^H \cos\left(\frac{z}{H} \cdot \frac{\pi}{2}\right) dz * 2\pi \int_0^R J_0\left(\frac{r}{R} \cdot \rho_0\right) r dr = 3GW$ shows that $Q'''_{pow_0} = 7.16 \cdot 10^8 \frac{W}{m^2}$.

To make sure that the nominal power of the MSFR is 3 GW, the boundaries of the power source are chosen just inside the core of the MSFR; H=0.75 and R=1.0.

3.2.3. Pump

Above the heat exchanger, there is a pump present in each of the sectors. This pump is simulated by imposing a volumetric momentum force $\frac{\Delta p}{H}$ on the volume and drives the molten salt circulation during nominal operation. In the simulations performed in this project the height of the volume H is 0.042m and the pressure difference Δp is $48.7 \cdot 10^3$ Pa [4].

3.2.4. Heat exchanger

The molten salt flows downwards in the heat exchanger, while the intermediate fluid flows upwards. The heat transfer to the intermediate circuit is simulated by the following equation:

$$P_{tr} = \gamma \, (T - T_{intermediate}) \tag{3.2}$$

In this equation, P_{tr} is the transferred power (per volume unity) to the intermediate circuit, γ is the volumetric heat transfer coefficient, T is the temperature of the fuel and T_{int} is the average temperature of the intermediate fluid. In reality, the heat from the fuel circuit is transferred to the intermediate circuit at a surface between the two [15]. Because the exact design of the heat exchanger is not yet known, the heat exchanger was simulated with a volumetric heat transfer coefficient γ of $8.31 \cdot 10^5$ W/m^{3}K[4].

3.2.5. Pressure drop

In the heat exchanger, the fluid loses energy because of a pressure drop. Because the individual channels through which the fluid flows are relatively small, the heat exchanger is the only place in the fuel loop where the pressure drop cannot be neglected. In order to model the pressure drop in the heat exchanger, the Darcy friction factor f_d had to be determined. The shape of the heat exchanger channels for which the simulations were performed is presented in Figure 3.5 [15]. The shape of the channels influences the relation between the channel diameter and its hydraulic diameter. In the simulations performed in this project, the channel diameter was chosen at 2.0mm, which corresponds to a hydraulic diameter of 1.2mm.

Figure 3.5: Shape of channels in the heat exchanger that was used for the simulations [15].

For heat exchanger channels with a hydraulic diameter of around 1mm, the molten salt flow normally remains in the laminar region (the Reynolds number is dependent on the hydraulic diameter of the channels). For laminar flows in the heat exchanger, the friction factor f_d is defined as $4 \cdot \frac{15.78}{Re}$. The Reynolds number in the heat exchanger channels was approached by using the predicted average temperature and flow velocity of the molten salt, which resulted in a value of 399. Hence, the hydraulic diameter of 1.2mm that was chosen for the simulations results in a friction factor f_d of 0.158.

3.3. Simulations

For the project the following situation was simulated: while the MSFR is in steady-state nominal operation, all of the pumps break down. At the same time, the reactor is shut down, which means that the power is reduced to 6% of its value at nominal operation. In reality, the power gradually decreases to zero from this point, but in the experiment the power is kept at 6%. The heat exchanger keeps operating: the experiment is performed for the situation where only the pumps breaks down. From the point where the pumps are out of order the flow and the temperature distribution of the molten salt are studied over time.
The simulation described above was performed for three different heights of the heat exchanger; the original geometry, an elevation of 13 cm and a reduction of 13 cm. The different experiments should provide insight into the natural circulation capability of the MSFR and how it is influenced by the height of the heat exchanger. In Figure 3.6, the three different meshes used for the experiment are presented.

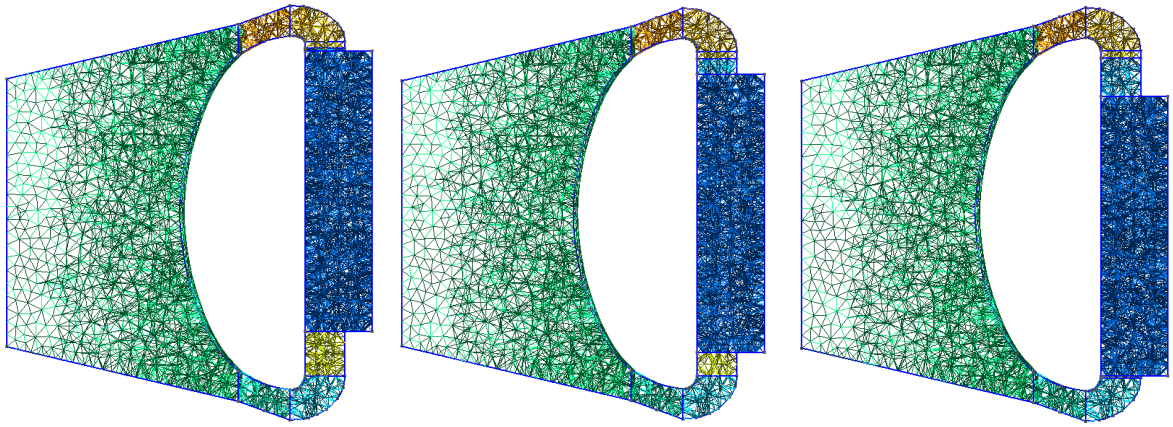

(a) HX elevated 13 cm (b) Normal geometry (c) HX lowered 13 cm

Figure 3.6: The different meshes on which the experiment has been performed.

4

Lowering temperature investigation

In this chapter, some unexpected behaviour of the power source is described. Although this problem was overcome in the end, it caused three weeks of delay to the project.

4.1. Lowering temperature in the fuel loop

In the experimental method it is explained that the kinematic viscosity of the molten salt was multiplied with a factor 10^4 to keep the flow in the laminar region. At the beginning of the experiment this was the only adapted molten salt property, which meant that the Prandtl number was a factor 10^4 too high. When the power source of equation 3.1 was imposed on the fuel circuit, the simulation seemed to be running well for the first few seconds. However, for longer running times the minimum temperature kept dropping until it got below the melting temperature of the molten salt. The first options that were chosen to solve this problem were running the tests with a lower viscosity, a smaller γ for the heat exchanger and smaller time steps. When these measures did not solve the problem, the imposed power source was investigated further.

4.2. Tests on a cylinder

To find out if the problem of the dropping molten salt temperature was in the power source, some tests have been performed on an isolated cylinder filled with molten salt. Because no heat could escape from the cylinder, and the power source was supposed to only add heat, the molten salt should not cool down anywhere. However, the minimum temperature of the molten salt was dropping, and for longer running times it eventually got below the melting temperature. Because the same problem was also happening if the code was solving for the enthalpy only (no fluid flow), the problem seemed to be in the power source.
After it was clear that the power source caused the minimum fluid temperature to drop, it was investigated at what location in the fluid this was happening. By doing different tests with different boundaries of the power source, we proved that the fluid temperature was dropping just outside the boundary of the power source. This is illustrated in Figure 4.1. Furthermore, the temperature of the fluid was not dropping if the boundaries of the power source were defined outside the cylinder. From these results it was concluded that the problem of the dropping fluid temperature was caused by inexplicable behaviour at the boundaries of the imposed power source.

4.3. Power source problem investigation

Several things were tried to solve the problem:

1. Changing the implementation of the power source. A small term was added to the power source to test if the problem would be happening because of a linearization at the boundary of the power

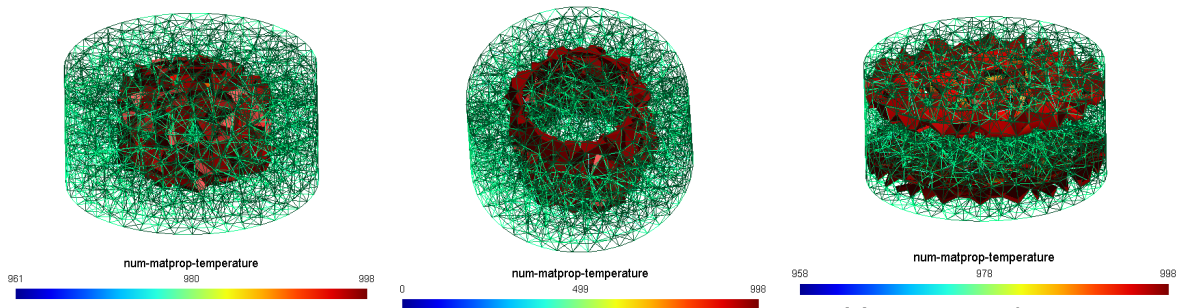

(a) r=1.0m and z=0.5m (b) r=2.0m and z=0.5m (c) r=1.0m and z=1.2m

Figure 4.1: Results of tests (after 3 seconds of running time) with three different power source boundaries imposed on an isolated cylinder filled with molten salt. The cylinder has a height of 2m, a radius of 1m and the r=0 and z=0 point is located in the m]iddle of the cylinder. The region where the temperature has dropped compared to the starting temperature is colored red. It can clearly be seen that this region matches with the boundaries of the power source.

source. In order to prevent the minimum temperature from dropping an unreasonably large term had to be added to the power source, which meant that this was no solution to the problem;

2. Changing the cosine and the Bessel function of equation 3.1 into constant functions to test if the problem would be in the coding of the power source itself;
3. Increasing the number of quadrature points and the order of approximation;
4. Imposing the power source on different 3D meshes filled with hexahedra and on 2D meshes;
5. Imposing different boundary conditions on the walls of the mesh. Instead of making the walls adiabatic they were assigned a minimum temperature;
   Measures 2, 3, 4 and 5 all did not change anything to the problem. This showed that the problem had to be somewhere else.
6. Making a mesh of several adjacent volumes with no physical boundary between them. Impose a constant heat source on only one of the volumes. For this case the same problem occurred at the boundary between the different volumes. This is illustrated in Figure 4.2;

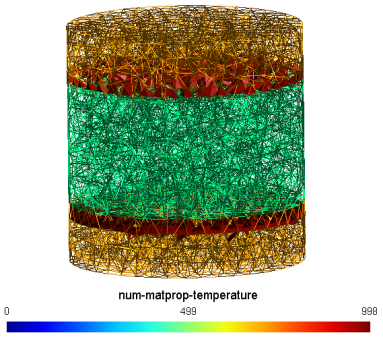

Figure 4.2: The only physical boundaries of this cylinder are on the outside. A constant heat source with its boundaries outside of the cylinder is imposed on only the green part of the cylinder. The region where the temperature has dropped compared to the starting temperature is colored red. It can be seen that in this case the problem is not happening at the boundaries of the power source itself but at the boundaries where it can work.

7. Increasing the heat conductivity with a factor 10^4 to get a realistic Prandtl number. This did not solve the problem, but the result was different from the ones in Figure 4.1. The fluid was still cooling down at the boundaries of the power source, but this cooling got diffused through the cylinder more quickly than with the previous experiments. This caused the minimum temperature to cool down less quickly. The result is illustrated in Figure 4.3.

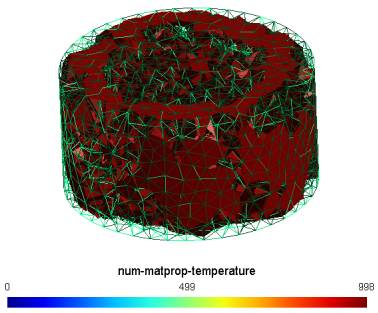

Figure 4.3: The same experiment as in Figure 4.1, only now with different material properties of the molten salt. The heat conductivity is increased with a factor 10^4, which results in a Prandtl number that has the same value as the real salt. It can be seen that the problem is still occurring, but that the cooling gets diffused more quickly.

4.4. Explanation of the problem

Although none of the tests solved the problem, they did give more insight into the problem that was happening. The problem is not a result of something that is coded wrong, but that it is a result of the Discontinuous Galerkin method. The change in temperature $\frac{dT}{dx} = \frac{q''}{\lambda}$ of the molten salt is dependent on its thermal conductivity λ. In DG methods the discrete functions do not have to be continuous between neighbouring elements, which means that the linearization of $\frac{dT}{dx}$ can cause the temperature to drop at the boundary due to an approximation error. If the λ is increased with a factor 10^4 the problem is reduced, which is expected because of the $\frac{1}{\lambda}$ dependence.
With an increased thermal conductivity λ of the molten salt, the simulations of the fuel circuit were able to reach nominal operation. This meant that the simulations could be performed as planned with the power source of equation 3.1. The results are described in the next chapter.

5

Results and Discussion

This chapter treats the results of the simulations that were performed. In the first section the temperature distribution and the flow velocity of the molten salt during nominal operation are described. Furthermore, the developments that occur if the pumps break down are discussed. The second section treats the influence of the heat exchanger on the natural flow capabilities of the fuel loop. Some discussion points are described in the third and final section of this chapter.

5.1. Normal geometry

5.1.1. Nominal operation

The temperature distribution and the fluid flow velocity during nominal operation are shown in Figure 5.1.

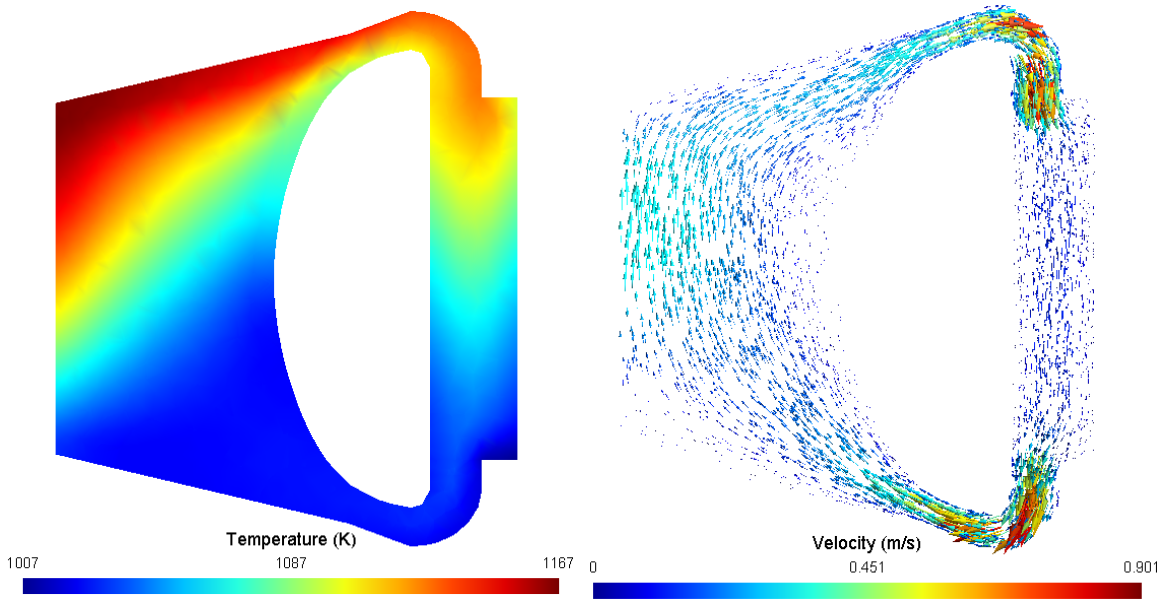

Figure 5.1: Molten salt temperature distribution (left) and flow velocity (right) during nominal operation.

In the SAMOFAR project, the core inlet temperature of the molten salt was chosen around 948K, after which it leaves the core around 1048K due to a temperature rise of 100K. In Figure 5.1 it can be seen that the in- and outlet temperatures of the core are respectively around 1020K and 1120K, which means that the temperature rise is reasonable but the temperatures themselves are too high. However, this is assumed to be due to the fact that the material properties of the molten salt in this simulations were not the same as those of the real molten salt. The temperature distribution in general corresponds to

what is expected from previous research.
Furthermore, in Figure 5.1 it can be seen that the flow is acting as expected. At the inlet and the outlet of the heat exchanger, the flow velocity increases, which is a reasonable result because the flow velocity should he higher at relatively narrow places to keep the system in steady-state. However, the maximum simulated flow velocity of 0.9 m/s is lower than is expected in the real MSFR, which is mostly due to the adapted kinematic viscosity ν of the molten salt. Furthermore, the friction factor f_d that was used for the simulations corresponds to a realistic molten salt velocity and temperature. Because the flow velocity and temperature of the simulations both differ from their predicted values, the effect of the pressure drop causes some uncertainty in the results.

5.1.2. Natural flow investigation

In this section, the temperature distribution and the velocity of the fluid flow are studied over time from the moment the pumps stop operating and the power reduces to 6% of its nominal value. The flow development of the molten salt can be seen in Figures 5.2 and 5.3, while the temperature distribution is presented in Figure 5.4.

1-10s after reactor shutdown

The moment the pumps stop working and the reactor shuts down, the fluid almost stops flowing through the sectors completely for the first 5s. As can be seen in Figure 5.2, the fluid does mainly flow around inside of the core while its speed is decreasing rapidly. After 5s, it can be seen that the flow through the sector starts to reestablish itself slowly, and that the maximum flow velocity has already decreased to 0.068 m/s. After 10s, the maximum velocity has decreased further to 0.021 m/s, but the natural circulation through the sector has increased further.
In Figure 5.4 it can be seen that the temperature distribution changes during the first 10s. While the inlet and the outlet core temperature remain roughly the same, the region in the core where the fluid heats up (the yellow region) gets more horizontal. This can be explained by the fact that the velocity at which the molten salt enters the core from below has decreased. The flow starts to rely more on natural circulation driven by buoyancy forces instead of pump power.

10-100s after reactor shutdown

The flow starts to look again like the velocity distribution at nominal operation. However, it should be noted that in this time frame the maximum flow velocity has decreased with about 95% compared to nominal operation. Furthermore, the yellow line of the temperature distribution becomes even more horizontal and the molten salt core inlet temperature decreases.

100-300s after reactor shutdown

In this time frame the flow approaches a new equilibrium. The core inlet and outlet temperatures decrease to respectively 925K and 1125K, while the core temperature rise ΔT increases to roughly 200K. This increase can be explained by the fact that the fluid spends a longer time in the reactor core before it enters the heat exchanger than during nominal operation.
However, it should be noted that the longer the experiment runs, the more inaccurate the results get. This is caused by the fact that the power is kept constant at 6% from the moment the pumps break down and the reactor is shut down. In reality, the power gradually decreases to zero after reactor shutdown, and reaches a value of around 3% of nominal operation power after 100s. Nevertheless, if the MSFR is able to cool itself down at 6% of the nominal power it will for sure be able to do this if the power decreases further over time.

Natural circulation capabilities

From the simulations it can be concluded that the MSFR is able to cool itself down in case the pumps stop working (*Note: this only applies if the reactor is shut down at the same moment*). In the first five seconds after the accident the flow is disturbed, but the flow gradually reestablishes itself through natural circulation. Overheating of the fuel loop does not occur, the maximum fluid temperature does not even increase after the pumps stop working.

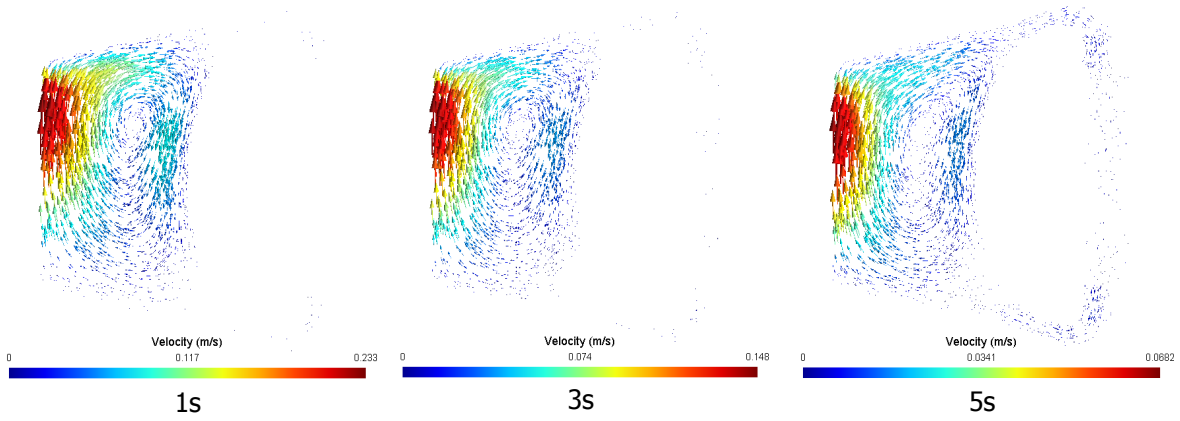

Figure 5.2: Flow development from the moment the pumps stop working and the reactor shuts down. *Note: Because the flow velocity decreases rapidly during the first 5 seconds all figures have their own velocity scales.*

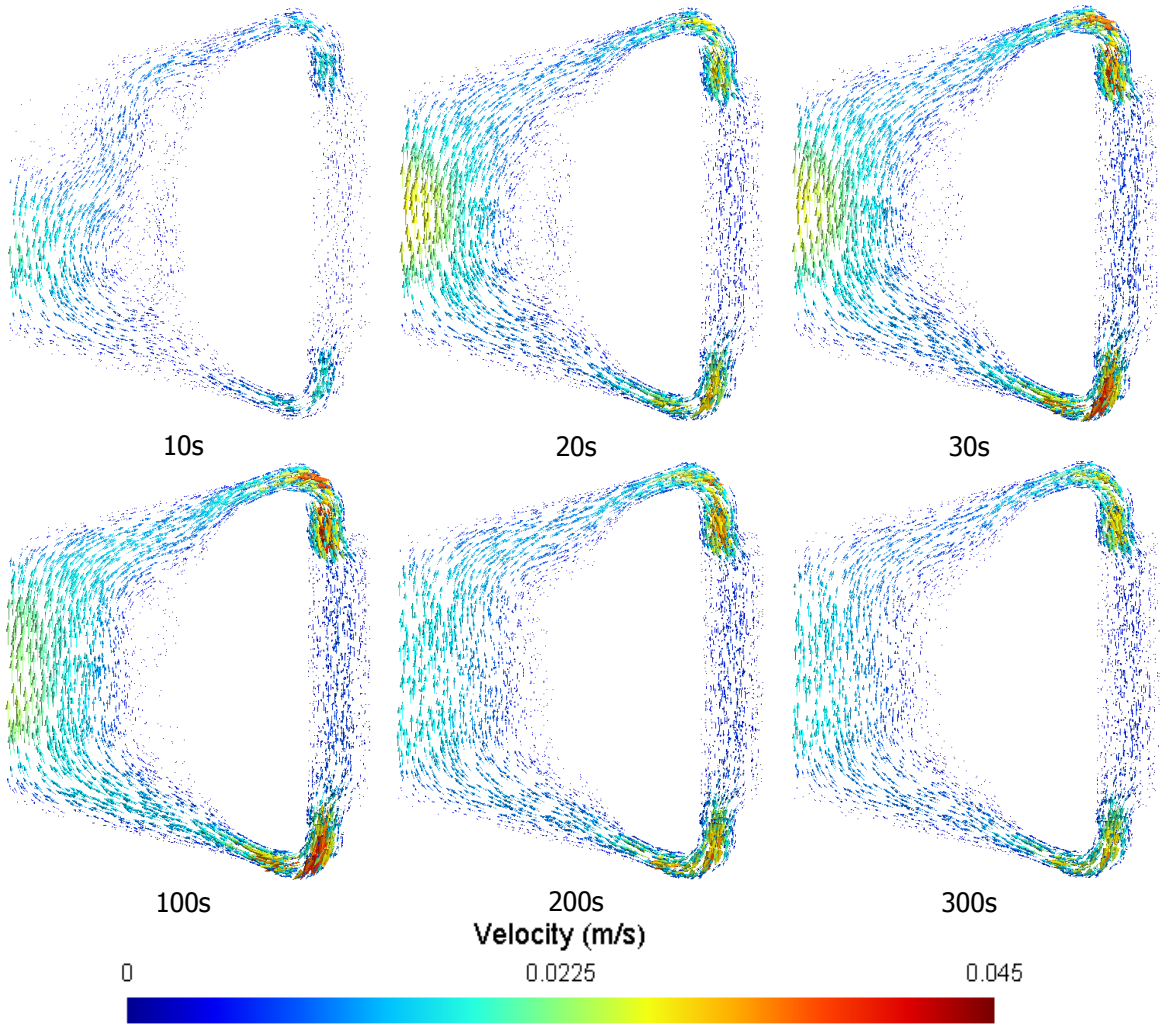

Figure 5.3: Flow development from 10s after the pumps have stopped working and the reactor has shut down. *Note: Because the flow velocity has stabilized from this point all of the figures have the same velocity scale.*

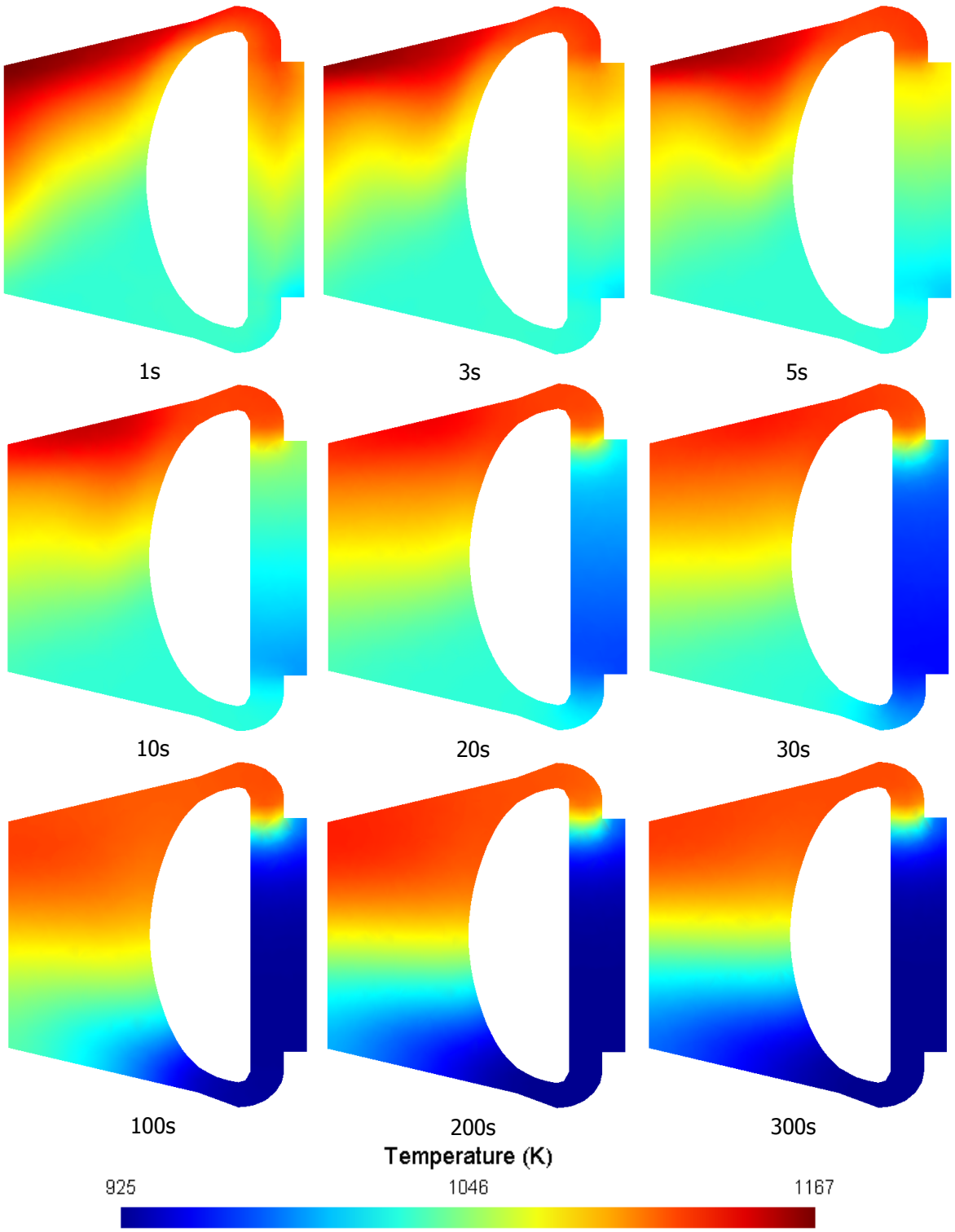

Figure 5.4: Temperature development from the moment the pumps stop working and the reactor shuts down. The scale values match with the minimum and maximum temperatures of the molten salt in this timeframe.

5.2. Different heat exchanger heights

In this section, the natural flow capabilities are compared for different heights of the heat exchanger. It can be seen in Figure 5.5 and Table 5.1 that during nominal operation the temperature distribution and the flow velocity are nearly identical for the different heat exchanger heights.
In Table 5.2, it can be seen that 30s after the moment the pumps stop working, the maximum flow velocity in the geometry with the high heat exchanger is 0.0435 m/s, while this is 0.0376 m/s in the low heat exchanger geometry. These maximum velocities are respectively 0.0451 m/s and 0.0396 m/s after 100s. This means that the difference in maximum flow velocity between the high and the low heat exchanger geometry are 14.5% and 13.0% for respectively 30 and 100s after the pump breaks down. However, this procentual difference is not representative for the difference in flow speed in the fuel loop in general. It can be seen in Figures 5.6 and 5.7 that this difference in natural circulation velocity occurs mainly in the regions just above and just below the heat exchanger. If the difference in maximum flow velocity is considered at the center of the core instead of in the whole fuel loop, the procentual differences between the high and the low heat exchanger geometries are smaller; 3.8% and 7.5% for respectively 30s and 100s after the pumps break down.
The slight differences in flow velocities between the different geometries do not result in significant temperature difference 30s after the pumps have broken down. In Table 5.2 it can be seen that the maximum difference in temperature is 0.2K. After 100s the differences in flow velocity have resulted in slightly higher temperature differences; the maximum temperature of the molten salt is 1119.6K for the elevated heat exchanger and 1123.1K for the lowered heat exchanger. However, this 3.5K difference is still negligible in terms of safety and in reality this difference will be even smaller because of the decreased power production.
The simulations have shown that in- or decreasing the heat exchanger height with 13cm does not have a significant impact on the natural cooling capabilities of the MSFR.

5.3. Discussion points

For reliable results that prove reactor safety the experiment should be redone with realistic molten salt properties once the DG-Flow code is able to handle turbulence. A turbulent flow of the molten salt could lead to new insights that influence the reactor safety. Furthermore, the adapted molten salt properties caused a higher temperature during the simulations than the molten salt will have in reality. Besides the fact that this does not result in a veracious simulation, the validity range of the calorific capacity of the molten salt of table 3.1 is exceeded.

Both the values for the volumetric heat transfer coefficient γ and the pressure difference Δp for the simulation of the pump have been taken from a previous thesis [4]. However, for that thesis different molten salt material properties and temperatures were used than for this project. Furthermore, the simulated pump was imposed on a region with a height of 0.042m above the heat exchanger. These are not the exact location and size of the pump that will be included in the real MSFR.

Because the design of the heat exchanger is not known yet, a volumetric heat transfer coefficient γ with unit [W/(m^3· K)] was imposed. However, the experiment would have been more accurate if the real geometry with the real heat transfer coefficient with unity [W/(m^2· K)] was used.

Finally, the problem that was described in chapter 4 was still occuring during the experiment. Although its effect got smaller when the experiment was performed with molten salt with the right Prandtl number, it was still influencing the results.

Table 5.1: Temperature and velocity distribution during nominal operation. The maximum and minimum temperatures in the fuel loop are presented in the left two columns. In the two right columns the maximum velocity in the fuel loop and in the center of the core are shown.

	Max. T (K)	Min. T (K)	Max. v (m/s)	Max. v in center of the core (m/s)
HX high	1167.6	994.7	0.889	0.351
HX normal	1167.5	995.1	0.901	0.354
HX low	1167.4	995.1	0.902	0.354

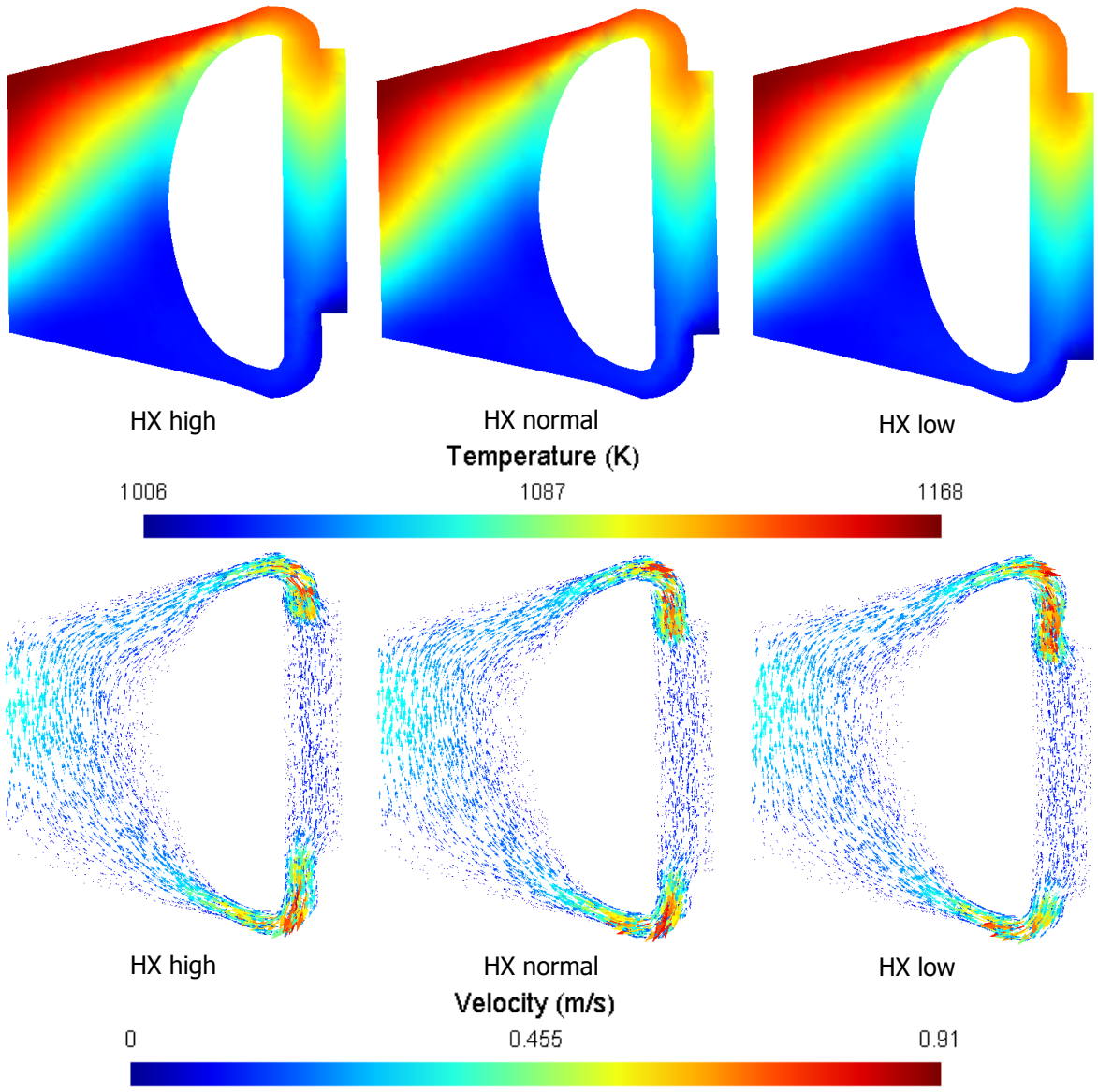

Figure 5.5: The temperature distribution and flow velocity during nominal operation for three different heights of the heat exchanger.

Table 5.2: Temperature and velocity distribution 30s after the pumps break down. The maximum and minimum temperatures in the fuel loop are presented in the left two columns. In the two right columns the maximum velocity in the fuel loop and in the center of the core are shown.

	Max. T (K)	Min. T (K)	Max. v (m/s)	Max. v in center of the core (m/s)
HX high	1131.5	951.5	0.0435	0.0265
HX normal	1131.3	951.5	0.0407	0.0261
HX low	1131.3	951.7	0.0376	0.0255

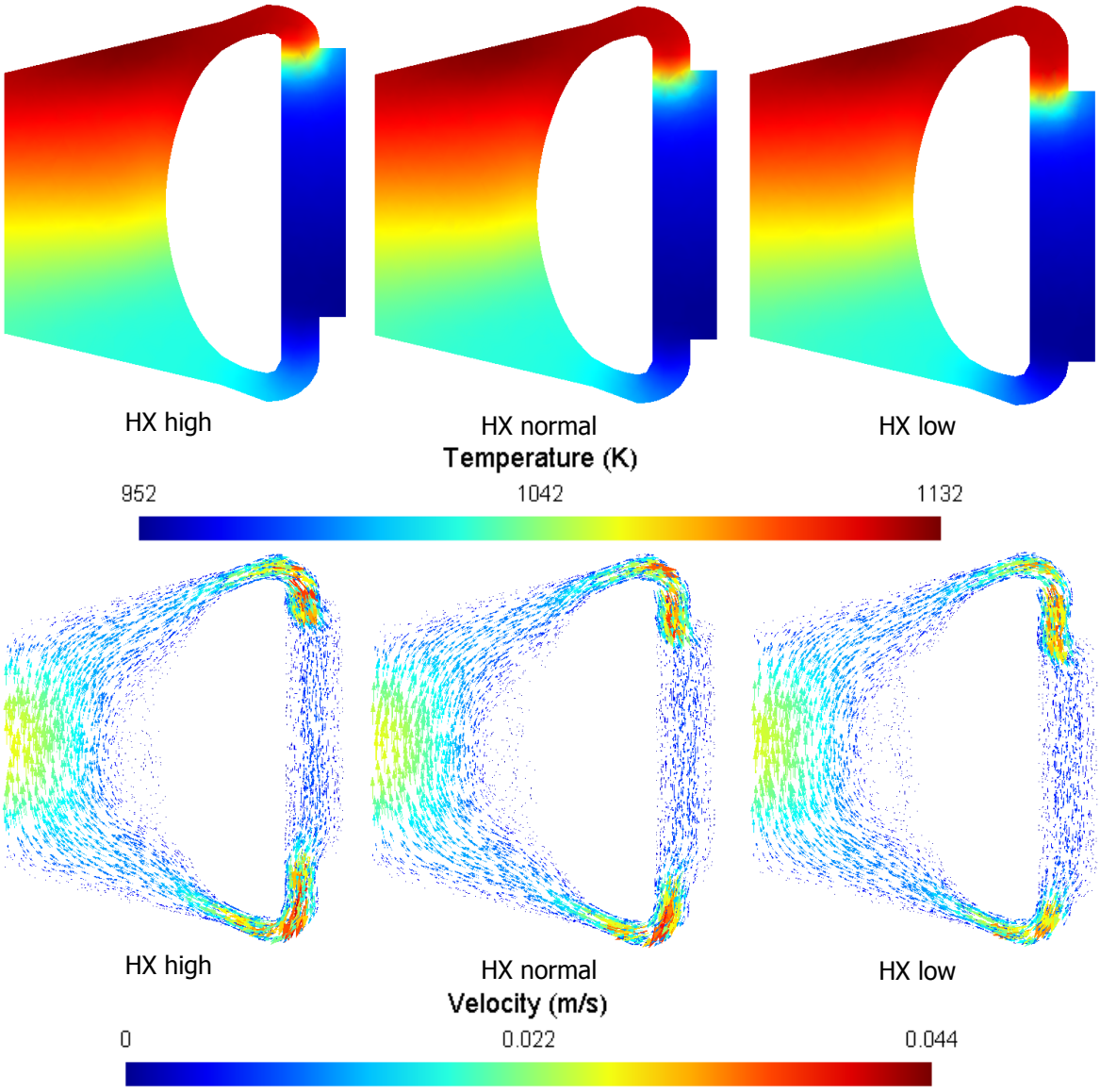

Figure 5.6: The temperature distribution and flow velocity 30 seconds after the pumps stop working for three different heights of the heat exchanger.

Table 5.3: Temperature and velocity distribution 100s after the pumps break down. The maximum and minimum temperatures in the fuel loop are presented in the left two columns. In the two right columns the maximum velocity in the fuel loop and in the center of the core are shown.

	Max. T (K)	Min. T (K)	Max. v (m/s)	Max. v in center of the core (m/s)
HX high	1119.6	926.2	0.0451	0.0248
HX normal	1121.2	926.2	0.0423	0.0240
HX low	1123.1	926.2	0.0396	0.0230

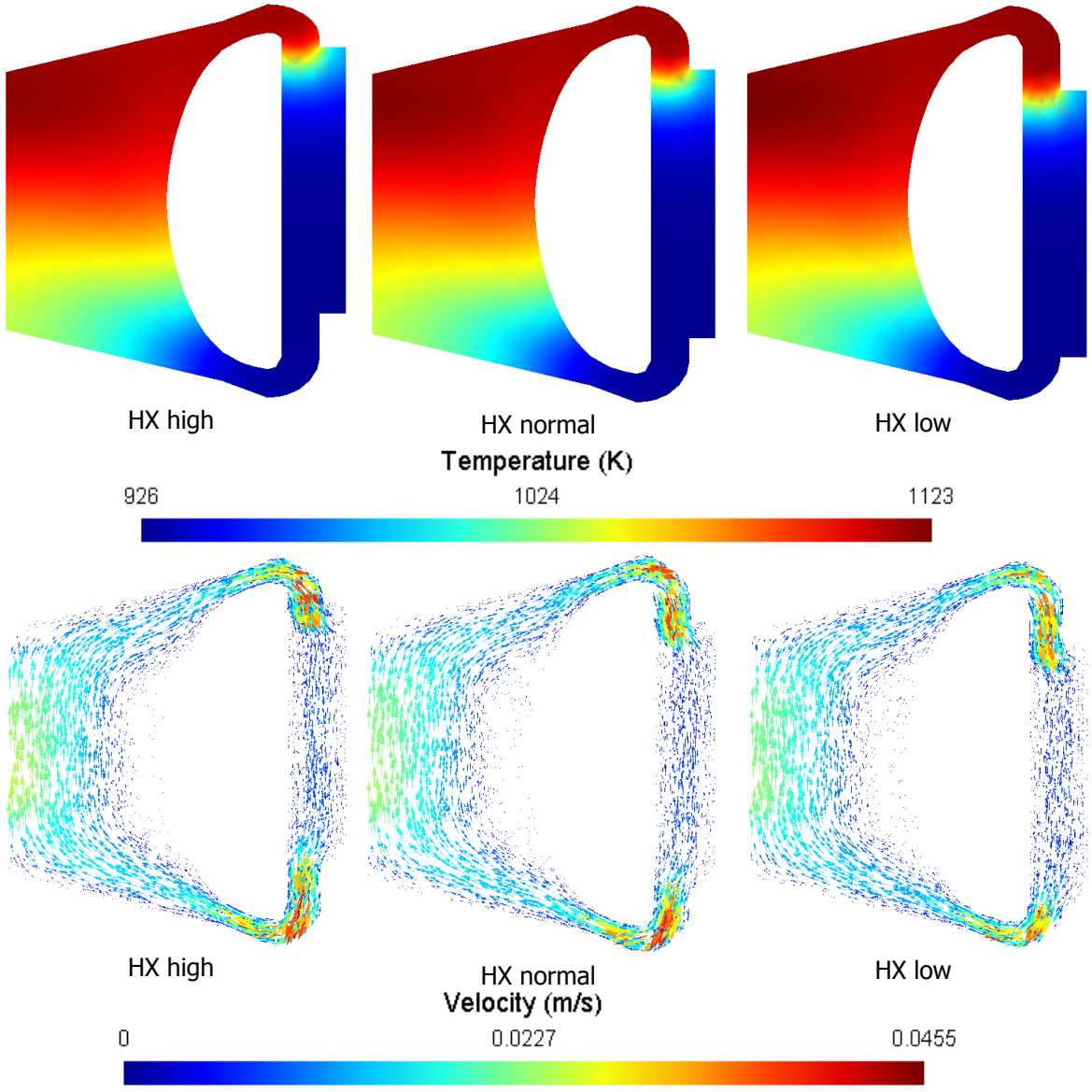

Figure 5.7: The temperature distribution and flow velocity 100 seconds after the pumps stop working for three different heights of the heat exchanger.

6

Conclusions

The outlined aim of this thesis was two-fold:

- To describe to what extent natural circulation is able to remove delayed heat production in case the pumps stop working;
- Furthermore, to describe the influence of the height heat exchanger on the natural circulation capabilities.

6.1. Approximation error

Before usable results could be obtained from the simulations, an error was encountered at the boundaries of the power source that simulates the generated heat of fission reactions. At this location, the temperature of the fluid was dropping unexpectedly, which was even happening if the power source was imposed on an isolated cylinder filled with molten salt. Further research into this problem led to the conclusion that it was the result of the Discontinuous Galerkin method. The linearization of the temperature change caused the temperature to drop at the boundary. Because the change in temperature has a dependence on $\frac{1}{\lambda}$, the problem was reduced by increasing the thermal conductivity λ of the molten salt with a factor 10^4. Nevertheless, it should be taken into account that the problem was still occurring during the simulations performed in this project.

6.2. Natural circulation capabilities

From the simulations, it can be concluded that the MSFR is able to cool itself down in case the pumps stop working and the reactor shuts down at the same moment. In the first 5s after the accident, the flow through the sectors is disturbed, but it gradually reestablishes itself through natural circulation. Overheating of the fuel loop does not occur, the maximum fluid temperature does not even increase after the pumps stop working.

6.3. Different heat exchanger height

An increased height of the heat exchanger slightly increases the natural flow capabilities of the MSFR. The difference in maximum flow velocity between the high and the low heat exchanger geometry are 14.5% and 13.0% for respectively 30 and 100s after the pump breaks down. However, this procentual difference is not representative for the difference in flow speed in the fuel loop in general, it occurs mainly in the regions just above and just below the heat exchanger. If the difference in maximum flow velocity is considered at the center of the core instead of in the whole fuel loop, the procentual differences between the high and the low heat exchanger geometries are smaller; 3.8% and 7.5% for respectively 30s and 100s after the pumps break down. However, these differences in flow velocity do not result in temperature differences of more than 3.5K between the geometries with different heights of the heat exchanger. Hence, the experiment shows that in- or decreasing the heat exchanger height with 13cm does not have a significant impact on the natural cooling capabilities of the MSFR.

6.4. Future research recommendations

During this thesis several topics were encountered that require further research:

- The experiment was performed with adapted molten salt material properties in order to keep the flow laminar. For reliable results that prove reactor safety the experiment should be redone with realistic molten salt properties once the DG-Flow code is able to handle turbulence;
- An investigation of the influence of the Darcy friction factors f_d on the natural circulation capabilities would lead to more insight into the requirements of the heat exchanger design;
- The simulation of the flow in the heat exchanger would provide more accurate results if it would be performed on a mesh containing the individual channels of the heat exchanger instead of a volumetric heat transfer coefficient;
- An investigation of the influence of the pump size and location in the fuel circuit on the flow capabilities;
- The tests that were done gave new insight into an approximation error due to the Discontinuous Galerkin method. For steep gradients in the imposed power the CFD code can give unrealistic results. The approximation error caused by the DG method needs further investigation to obtain more reliable results.

Bibliography

[1] GENTLE, DelftX. Nuclear Fission Reactor Principles, Light Water Reactor Systems and Safety and Next Generation Nuclear Power. *Understanding Nuclear energy - NUCLEAR01x.* Retrieved from: https://courses.edx.org/courses/course-v1:DelftX+NUCLEAR01x+1T2017/course/

[2] M. Allibert, D. Gerardin, D. Lathouwers et al. *Description of initial reference design and identification of safety aspects.* SAMOFAR Deliverable 1.1, EURATOM, 2016.

[3] M. Brovchenko, D. Heuer, E. Merle-Lucotte et al. *Design-Related Studies for the Preliminary Safety Assessment of the Molten Salt Fast Reactor* Nuclear Science and Engineering: The journal of the American Nuclear Society, 2013.

[4] E. Van der Linden. *Coupled neutronics and computational fluid dynamics for the molten salt fast reactor* Master Thesis, Section Physics of Nuclear Reactors, Delft University of Technology, 2012.

[5] *What is buoyant force?* Khan Academy. Retrieved from: https://www.khanacademy.org/science/physics/fluids/buoyant-force-and-archimedes-principle/a/buoyant-force-and-archimedes-principle-article

[6] A. Cammi, D. Lathouwers, M. Tiberga et al. *Dynamics in natural circulation loop for internally heated molten salt.* SAMOFAR Deliverable 3.2, EURATOM, 2017.

[7] H. Van den Akker, R. Mudde. *Fysische Transportverschijnselen.* Delft Acedemic Press, Leeghwaterstraat, Delft, The Netherlands, 2014.

[8] P.K. Kundu, I.M. Cohen. *Fluid Mechanics.* Fourth Edition, Acedemic Press, Elsevier, Oxford, 2008.

[9] S.V. Patankar. *Numerical Heat Transfer and Fluid Flow* Hemisphere Publishing Corporation, United States of America, 1980.

[10] A. Segal. *Finite element methods for the incompressible Navier-Stokes equations.* Delft University of Technology, Institute of Applied Mathematics, Delft, The Netherlands, 2006.

[11] K. Shahbazi. *A Parallel High-Order Discontinuous Galerkin Solver For the Unsteady Incompressible Navier-Stokes Equations in Complex Geometries.* Department of Mechanical and Industrial Engineering, University of Toronto, 2007.

[12] R. Hartmann. *Numerical Analysis of Higher Order Discontinuous Galerkin Finite Element Methods.* Institute of Aerodynamics and Flow Technology, DLR (German Aerospace Center), Braunschweig, Germany.

[13] C. Geuzaine and J.-F. Remacle. *Gmsh: a three-dimensional finite element mesh generator with built-in pre- and post-processing facilities.* International Journal for Numerical Methods in Engineering 79(11), pp. 1309-1331, 2009.

[14] M. Aufiero. *Development of advanced simulation tools for circulating-fuel nuclear reactors* Doctoral Dissertation, Department of Energy, Politecnico di Milano, 2014.

[15] A. Cammi, A. Di Ronco, S. Lorenzi. *Molten Salt Fast Reactor heat exchangers analysis.* SAMOFAR Deliverable 1.7, EURATOM, 2017.

[16] S. Wang, A. Rineiski, R. Li et al. *Safety Analysis – Transient Calculations* EVOL Deliverable 2.7, 2014.

[17] V. Ghetta, J. Giraud, P. Rubiolo, et al. *MSFR Fuel Salt Conditions During Typical Draining Transients* SAMOFAR Deliverable 3.1, EURATOM, 2017.